ARTICLE | Article in Press

Characterization of FLT3-ITD-mutated leukemic stem cells: functional and clinical insights

Serena Travaglini · Tiziana Ottone · Silvia Antonelli · Martina Serra · Giorgia Silvestrini · Silvia Masciarelli · Martyna Sniegocka · Nelida Ines Noguera · Marco De Bardi · Mirko Lomi · Maria Antonietta Irno Consalvo · Carmelo Gurnari · Rocco Piazza · Mariadomenica Divona · Francesco Marchesi · Francesco Fazi · Maurizio Mattei · Francesco Buccisano · Luca Battistini · Paola Guglielmelli · Alessandro Maria Vannucchi · Adriano Venditti · Daniela Francesca Angelini · Maria Teresa Voso

Received: 9 March 2026 / Revised: 1 August 2026 / Accepted: 19 August 2026
© The Author(s) 2026

Abstract

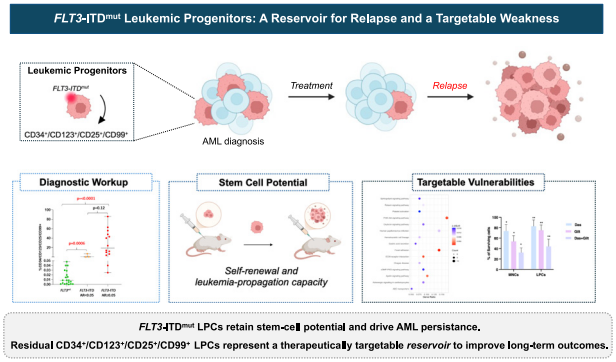
Despite treatment advances, relapsed/refractory *FLT3*-ITD-mutated acute myeloid leukemia (*FLT3*-ITD^{mut} AML) remains an unmet medical need. We previously identified a CD34/CD123/CD25/CD99+ leukemic progenitor cell (LPC) population that persists after induction treatment and drives disease recurrence in *FLT3*-ITD^{mut} AML. Here, we performed an integrated functional and molecular characterization of *FLT3*-ITD^{mut} LPCs. Multiparametric flow cytometry prospectively demonstrated that CD34/CD123/CD25/CD99+ expression levels above 7.4% robustly predict *FLT3*-ITD mutation with 88.2% sensitivity and 100% specificity. Sorted LPCs efficiently engrafted conditioned NSG mice and reinitiated leukemia, with sequential passages expanding the LPC compartment, consistent with their role as a disease reservoir. Transcriptomic profiling of 13 paired LPCs and blasts revealed upregulation of protein kinases, primarily lymphocyte-specific protein tyrosine kinase (LCK), a finding confirmed in 28 additional *FLT3*-ITD^{mut} samples. Gilteritinib reduced proliferation and FLT3-STAT5 signaling in *FLT3*-ITD^{mut} cells and LPCs. Additional LCK inhibition further attenuated FLT3/STAT5 activity, disrupted aberrant FLT3 localization, and downregulated ABC transporter-associated multidrug resistance. Notably, combining gilteritinib with LCK blockade enhanced its anti-leukemic activity, consistent with a cooperative effect of these pathways in sustaining *FLT3*-ITD^{mut} leukemic progenitors. These findings provide the first functional evidence that *FLT3*-ITD^{mut} LPCs maintain stem cell potential in vivo, refine clinically actionable leukemic immunophenotype for diagnosis and MRD monitoring, and uncover novel molecular vulnerabilities. Collectively, they support strategies to selectively eradicate residual *FLT3*-ITD^{mut} LPCs to improve long-term outcomes in AML.

This Article in Press is shared early to give you faster access to new research. It is citable and carries a permanent DOI. The final edited version will replace it automatically.

https://doi.org/10.1038/s41420-026-03319-0

Published online: 28 September 2026

Springer



Key points

- *FLT3*-ITD^{mut} leukemic progenitor cells retain stem cell properties and sustain AML persistence and propagation.
- Residual CD34^{+}/CD123^{+}/CD25^{+}/CD99^{+} leukemic progenitors constitute a targetable reservoir whose eradication may improve long-term outcomes in FLT3-ITD AML.

Introduction

Despite the introduction in clinical practice of specific inhibitors, the persistence of leukemic stem cells (LSCs) represents one of the major obstacles to cure *FLT3*-ITD mutated Acute Myeloid Leukemia (*FLT3*-ITD^{mut}AML), which remains an unmet medical need. Since the discovery of this mutation, several studies have attempted to identify specific surface and cytoplasmic markers aberrantly expressed on leukemic cells, with the goal of driving the development of innovative treatment strategies [1–3].

FLT3 represents one of the most frequently mutated genes in de novo AML, accounting for ~0% of all cases. Mutations include internal tandem duplications (ITDs) of the juxtamembrane domain and tyrosine kinase domain (TKD) mutations. *FLT3* mutations constitutively activate the FLT3 receptor, playing a crucial role in the control of cell proliferation, differentiation, and survival. Furthermore, *FLT3*-ITD^{mut} is a prognostic marker, despite its wide variability in terms of insert size, sites of the insertion, and the mutation load [4]. It has long been reported that the negative prognostic impact of *FLT3*-ITD^{mut}, associated with a high rate of disease recurrence, at least partly due to the persistence of *FLT3*-ITD^{mut}-expressing LSCs after initial AML treatment. Particularly, we previously reported that the CD34 + /CD123 + /CD25 + /CD99+ leukemic precursor cells (LPCs) phenotype predicts for *FLT3*-ITD mutation and disease recurrence [5].

The development of FLT3-targeted agents, such as midostaurin, gilteritinib, and quizartinib [6–8] significantly improved patient outcome, allowing re-classification of *FLT3*-ITD^{mut} AML from the ELN adverse into the intermediate risk group [8, 9]. Despite the promising results, the relapse rate remains high [9], highlighting the need for further understanding of mechanisms of resistance to targeted therapies.

The most common mechanism of resistance in *FLT3*^{mut} AML is the activation of alternative signaling pathways able to circumvent the effects of FLT3 inhibition. Indeed, it has been reported that several protein kinases, such as LCK [10] (lymphocyte-specific protein tyrosine kinase), a Src family kinase (SFK) may cooperate with oncogenic *FLT3*-ITD^{mut}, acting as positive regulators of FLT3 signaling and promoting leukemia transformation and resistance.

Our study aims at deep characterization of the *FLT3*-ITD^{mut} stem cell compartment, providing the rationale for effective combination therapies, and incorporate novel biomarkers related to dynamic acquisition of treatment resistance.

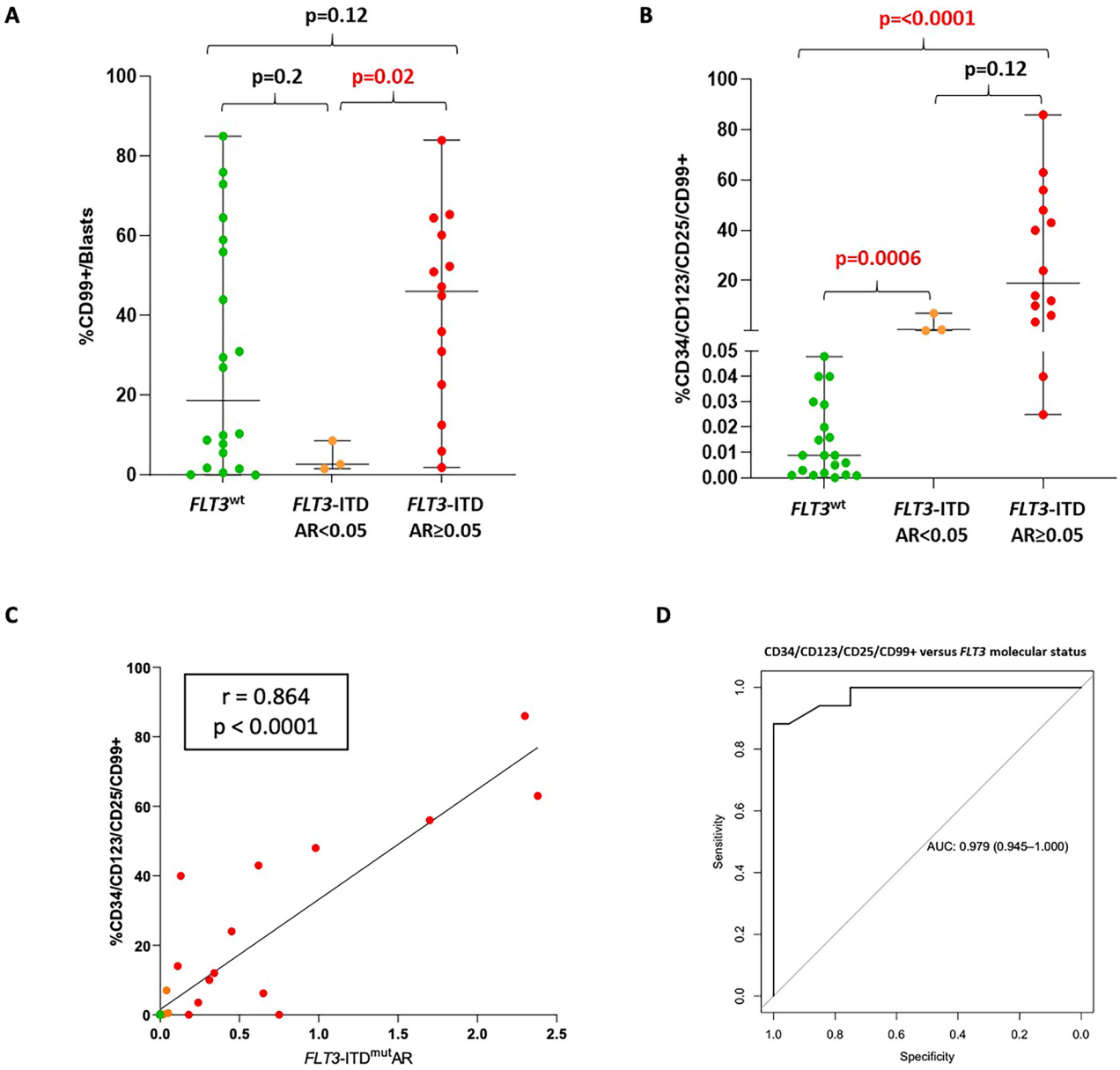


Fig. 1 Immunophenotypic and *FLT3*-ITD^{mut} analysis in AML samples. A Quantitative analysis of multiparametric flow cytometry (MPFC) data revealed no significant difference in the frequency of CD99+ cells within the blast population (CD34−/CD3−/CD19−/CD14−) between *FLT3*-ITD^{mut} ($n = 17$) and *FLT3*^{wt} ($n = 20$) samples. However, (**B**) analysis of the CD34 + /CD123 + /CD25 + /CD99+ population within the total CD34+ fraction showed a marked and statistically significant enrichment in *FLT3*-ITD^{mut} samples compared with *FLT3*^{wt} AML. Each dot represents an individual sample; horizontal lines indicate median values. Statistical significance was assessed using the Mann–Whitney test. **C** Spearman correlation analysis between the percentage of CD34 + /CD123 + /CD25 + /CD99+ cells within the total CD34+ fraction and the *FLT3*-ITD^{mut} allelic ratio (AR) measured in the bulk sample ($n = 17$), revealing a strong positive correlation ($r = 0.864$, $P < 0.0001$). **D** Receiver operating characteristic (ROC) curve is generated by plotting the variable mentioned above. The assay achieved a sensitivity of 88.2% and a specificity of 100% at the defined cut-off.

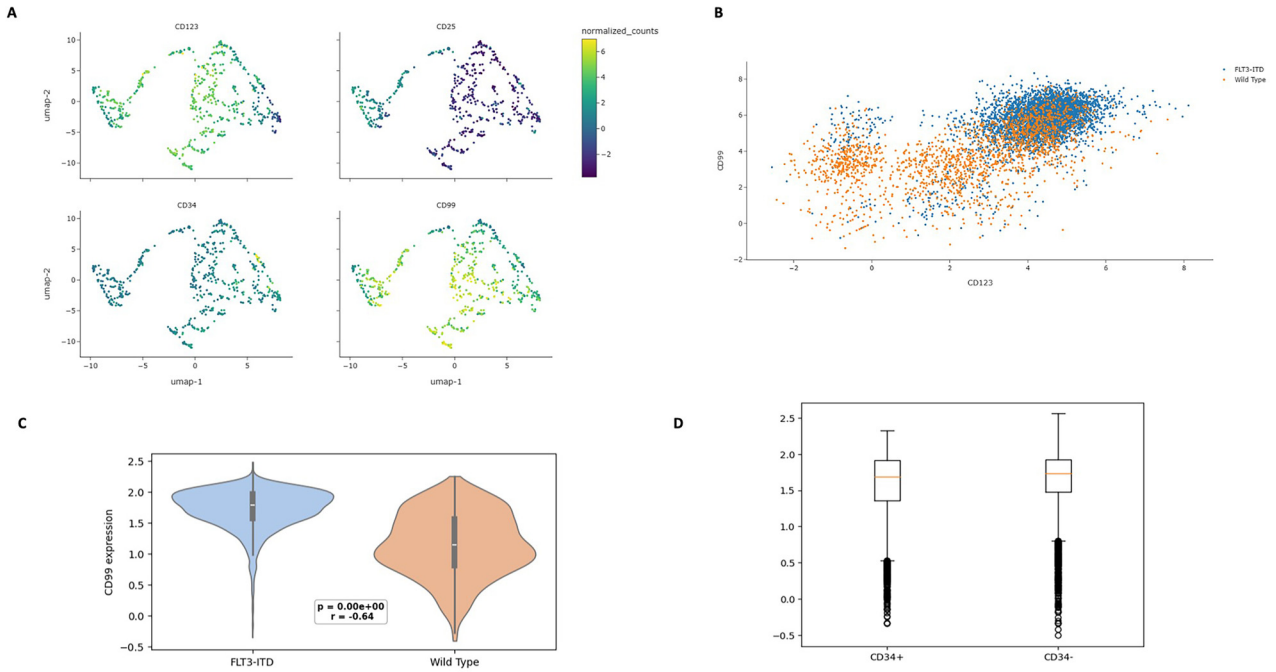


Fig. 2 Single-cell characterization of FLT3-ITD-mutated leukemic progenitor cells (LPCs). A UMAP plots from DAb-seq single-cell analysis of a BM sample (UPN31), illustrating normalized single-cell expression levels of CD34, CD123, CD25, and CD99 across individual cells. **B** Scatter plot showing the correlation between CD123 and CD99 expression at the single-cell level, with cells colored according to *FLT3*-ITD mutational status (blue: FLT3-ITD, orange: wild-type). **C** Violin plot showing the distribution of normalized CD99 expression in *FLT3*-ITD^{mut} versus wild-type cells, demonstrating significantly higher CD99 expression in *FLT3*-ITD-mutated versus wild-type cells. **D** Box plot comparing CD99 expression between CD34+ and CD34- cell subsets, showing comparable CD99 levels across both fractions. Statistical comparisons were performed using the Mann–Whitney test.

Results

The CD34 + /CD123 + /CD25 + /CD99 + LSC phenotype is predictive for FLT3-ITD^{mut} AML

To test the applicability of the CD34 + /CD123 + /CD25 + /CD99 + LSC-associated phenotype in the diagnostic workup of AML, we prospectively analyzed primary BM AML samples at diagnosis. Out of 37 tested samples, 14 (37.8%) were *FLT3*-ITD^{mut} (median AR = 0.54, range 0.11–2.38), 3 (0.8%) were characterized by a *FLT3*-ITD^{mut} micro-clones (median AR = 0.02, range 0.01–0.04), while 20 were *FLT3* wild-type (*FLT3*^{wt}). Multiparametric flow cytometry (MPFC) analysis revealed no significant difference in the frequency of CD99+ cells within the blast population between *FLT3*-ITD^{mut} (median 46.15, range 1.9–84) and *FLT3*^{wt} (median 18.7, range 0.001–85) samples, indicating that CD99 frequency alone is not sufficient to discriminate *FLT3* mutational status (Fig. 1A). In contrast, a statistically significant enrichment of the LSC phenotype (CD34 + /CD123 + / CD25 + /CD99 +) was observed in *FLT3*-ITD^{mut} patients (median 19%, range 0.025–86%, $P < 0.0001$) vs *FLT3*^{wt} (median 0.009%, range 0.0001–0.048%) (Fig. 1B), when calculated within the total CD34+ compartment. Moreover, we found a direct correlation between the percentage of CD34 + / CD123 + /CD25 + /CD99+ cells within the total CD34+ fraction and the *FLT3*-ITD^{mut} allelic ratio (AR, $r = 0.864$, $P < 0.0001$, Fig. 1C). As shown in Fig. S4A, B, our gating strategy for this LAIP was also able to detect *FLT3*-ITD^{mut} micro-clones within the leukemic population. The value >7.4% CD34 + /CD25 + /CD123 + /CD99+ cells was identified as the optimal threshold for predicting *FLT3*-ITD^{mut} by a Receiver operating characteristic (ROC) curve analysis (Fig. 1D). At this cut-off, the assay achieved 88.2% sensitivity and 100% specificity. The area under the ROC curve (AUC) was 0.98 (95% CI: 0.94 –1.00; $P < 0.0001$), indicating an excellent discriminative performance.

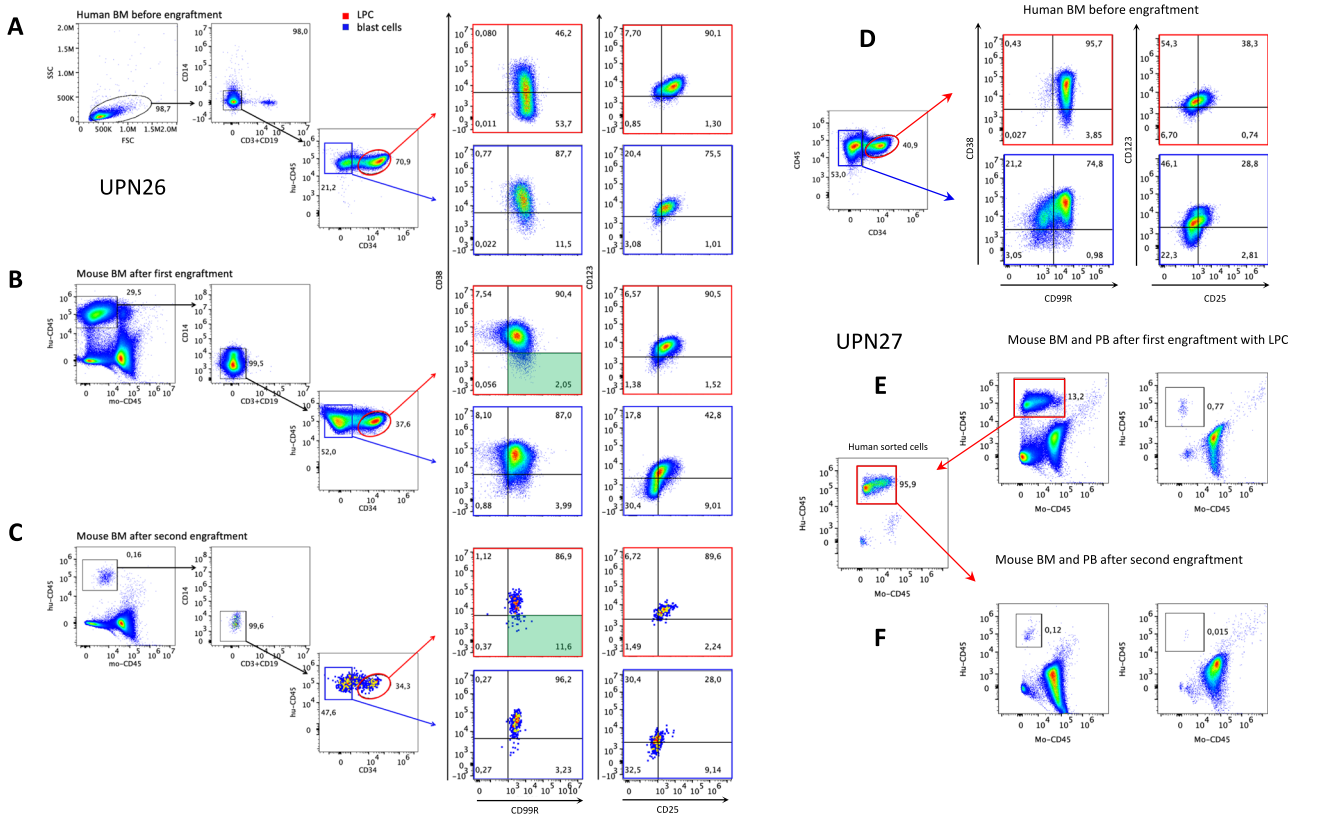


Fig. 3 Representative serial xenotransplantation experiments demonstrating the leukemia-initiating capacity of *FLT3*-ITD^{mut} LPCs. Representative serial xenotransplantation experiments performed using bone marrow (BM) samples from two *FLT3*-ITD^{mut} AML patients, UPN26 (**A**–**C**) and UPN27 (**D**–**F**). **A**, **D** Representative flow cytometry plots showing the sorting strategy used to isolate *FLT3*-ITD^{mut} LPCs and the immunophenotypic characterization of the sorted cells prior to transplantation. **B** Representative first engraftment of LPCs from UPN26. Flow cytometry plots show the percentage of human leukemic cells detected in the bone marrow (BM) of recipient mice together with the immunophenotypic characterization of the engrafted human cells. **C** Representative second (serial) engraftment of UPN26-derived LPCs. The percentage of human leukemic cells detected in the BM of secondary recipient mice and the immunophenotypic profile of the engrafted cells are shown. **E** Representative first engraftment of LPCs from UPN27 showing the percentage of human CD45$^+$ leukemic cells detected in the BM and PB of recipient mice. **F** Representative serial transplantation experiment using UPN27-derived LPCs. Post-sort purity of human cells isolated from primary recipient mice prior to secondary transplantation is shown, together with the percentage of human CD45$^+$ leukemic cells detected in the BM and PB of secondary recipient mice.

The positive and negative predictive values (PPV and NPV), calculated using the 7.4% threshold, were 100% and 95.8%, respectively. These data confirm that the proportion of CD34 + /CD123 + /CD25 + /CD99+ cells represents a robust marker to identify *FLT3*-ITD^{mut} AML with high accuracy.

To gain insights into the molecular and phenotypic determinants of *FLT3*-ITD^{mut} LSCs, single-cell analyses were performed on a primary *FLT3*-ITD^{mut} AML BM sample (UPN31). Consistently, UMAP visualization confirmed the presence of a distinct cluster (Fig. 2A), with strong co-expression of CD123 and CD99, enriched within the *FLT3*-ITD^{mut} fraction (Fig. 2B). Comparative single-cell analysis showed significantly higher normalized CD99 expression in *FLT3*-ITD^{mut} cells compared with wild-type counterparts (Fig. 2C). In contrast, comparable CD99 expression levels were observed between CD34+ and CD34- leukemic subsets (Fig. 2D), suggesting that CD99 marks a broader leukemic progenitor compartment beyond the primitive CD34+ cells.

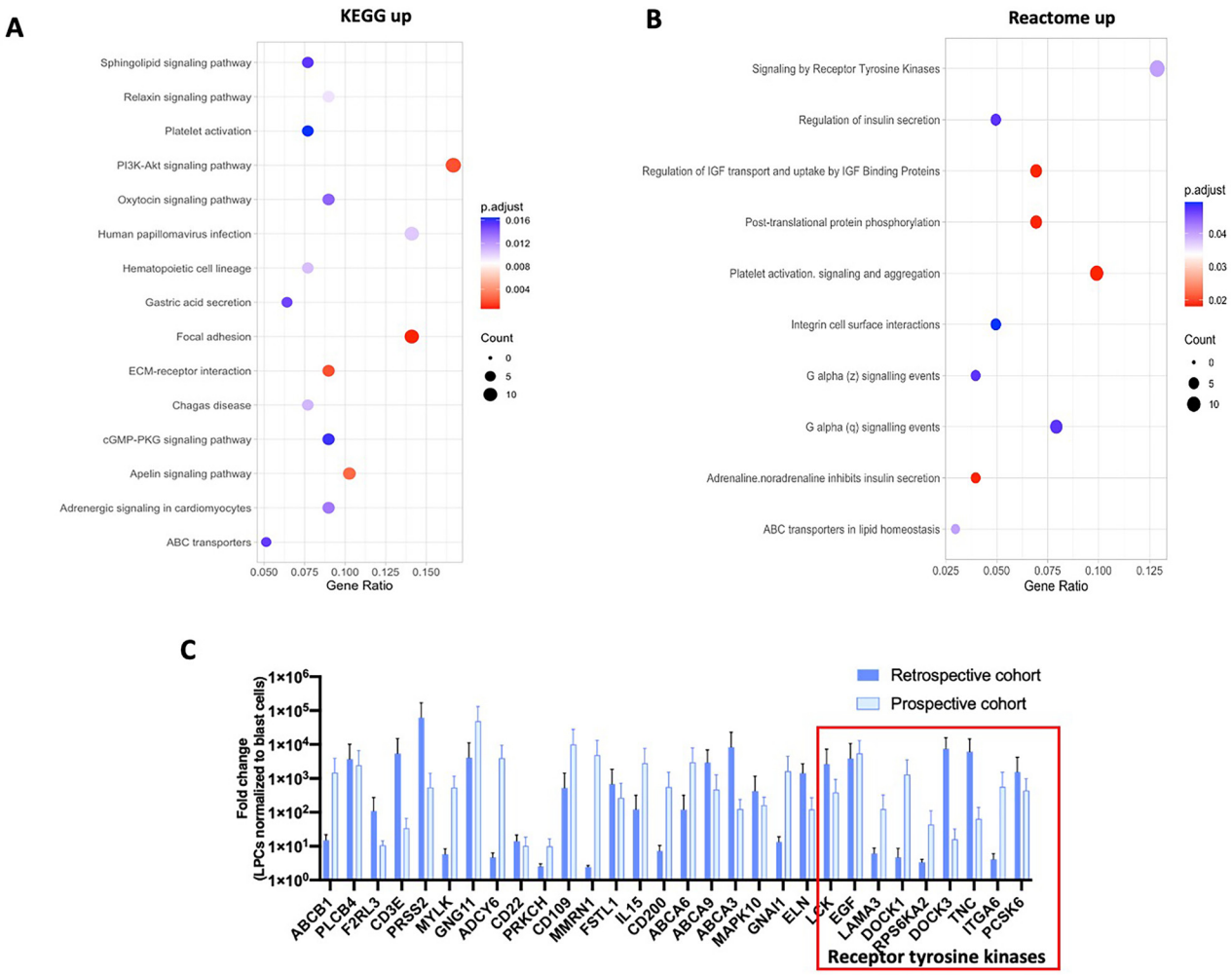


Fig. 4 Transcriptome profiling and pathway enrichment in *FLT3*-ITD^{mut} LPCs versus leukemic blasts. A KEGG pathway analysis and **B** Reactome pathway analysis based on the DAVID bioinformatic tool in 13 paired *FLT3*-ITD^{mut} LPC versus blast samples. Bubble color and size reflect *P*-adjusted and count values, respectively. **C** Validation of RNA-Seq results by TaqMan gene expression array in both a retrospective ($n = 3$) and prospective ($n = 3$) study cohort, indicated as empty columns. Fold change = 2-ΔΔCt; 2-ΔΔCt =2-(ΔCt LPCs - ΔCt BLASTS); ΔCt = Ct test gene – Ct housekeeping gene; housekeeping gene = GAPDH. Data are presented as median with range. Statistical significance was assessed using the Wilcoxon matched-pairs signed-rank test.

LPCs are capable of engrafting and re-initiating leukemia in NSG mice

To functionally assess the stem cell potential of *FLT3*-ITD^{mut} LPCs, *FLT3*-ITD^{mut} BM-MNCs were sorted into paired CD34 + /CD123 + /CD25 + /CD99+ LPCs and blasts (CD34−/CD3−/CD19−/CD14−/CD117 + /CD99 + /−), and individually transplanted into recipient busulfan-conditioned NSG mice ($n = 44$). A schematic representation of the experimental workflow is provided in Figs. S2 and S3. Given the variability in LPC frequency in different patient samples [11], we selected samples with LPCs proportion equal to or over 40% of the total CD45+ cells. Following transplantation of a median of 0.5×10^6 cells (range $0.3–1 \times 10^6$ cells), engraftment was observed in 19 of 29 NSG mice transplanted with LPCs (66%), with a mean time to engraftment of 4.5 ± 2.26 months from transplant (Figs. 3 and S5A). Engraftment levels, expressed as the percentage of hCD45+ cells in BM and PB from all successfully engrafted recipient mice, are reported in Fig. S5B. Representative flow-cytometric analyses of BM and PB samples from engrafted recipient mice demonstrated persistence of the specific CD34/CD123/CD25/CD99+ leukemia-

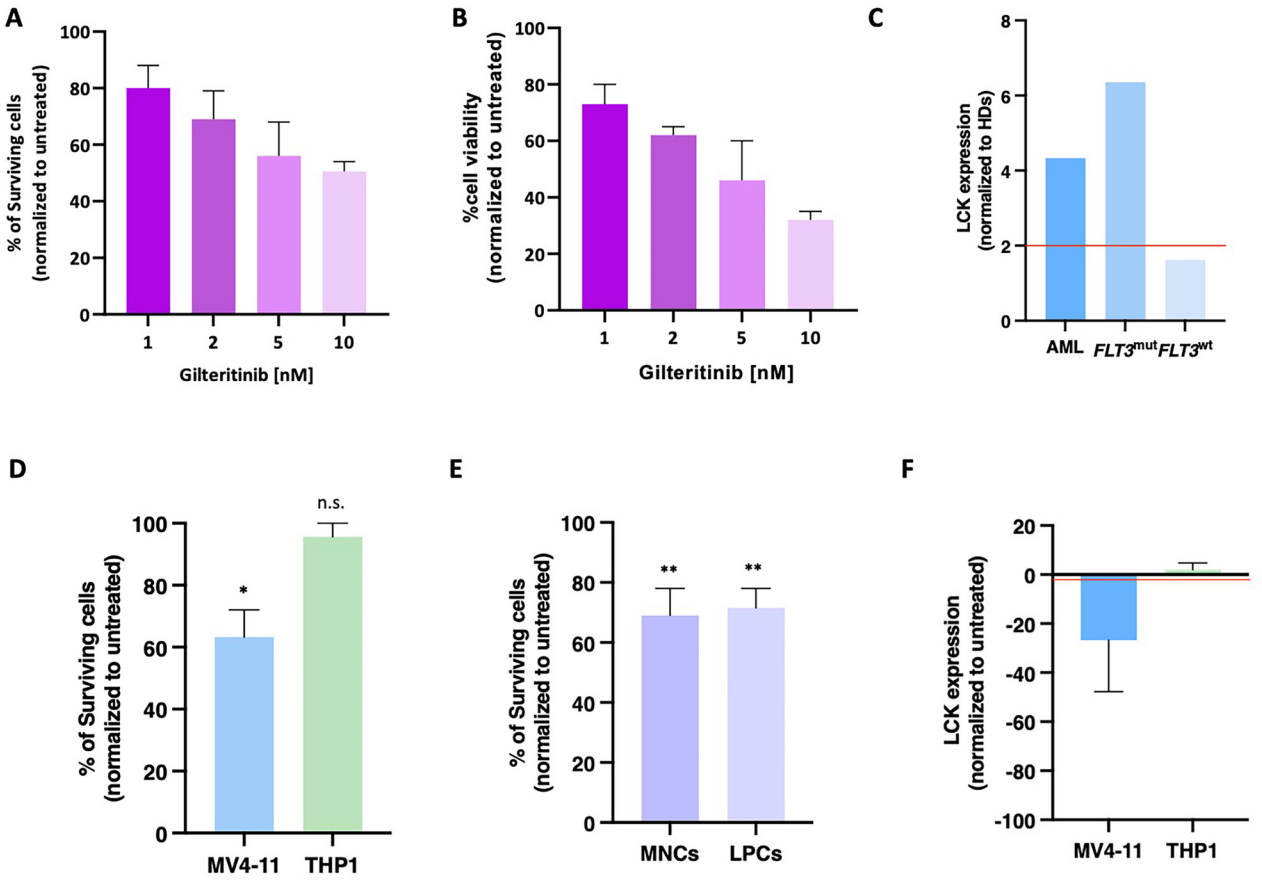


Fig. 5 LCK expression in *FLT3*-ITD^{mut} AML and functional impact of dasatinib treatment. Viability of MV4-11 cells evaluated after treatment with increasing concentration of Gilteritinib, for 24 h, using **A** Trypan-Blue dye exclusion assay and **B** MTS. Data are presented as median with range. Statistical significance was assessed using the Kruskal–Wallis test followed by Dunn's multiple-comparison test. **C** LCK expression evaluated by SYBR Green qRT-PCR in MNCs from *FLT3*^{mut} AML ($n = 35$), *FLT3*wt AML ($n = 25$), and healthy donor ($n = 8$) samples. The significant fold change cut-off is depicted with dashed red lines on the y axis. Statistical significance was assessed using the Kruskal–Wallis test followed by Dunn's multiple-comparison test. **D** Bar plot illustrating the percentage of surviving *FLT3*-ITD^{mut} MV4-11 and *FLT3*wt THP1 cells, after treatment with dasatinib for 72 h, using Trypan Blue staining. Values are normalized to the corresponding untreated control; statistical significance was calculated relative to untreated cells. **E** Bar plot illustrating the percentage of surviving *FLT3*-ITD^{mut} MNCs ($n = 3$) and LPCs ($n = 3$), after 72 h of treatment with dasatinib 100 nM, using Trypan Blue staining. Values are normalized to the corresponding untreated control; asterisks indicate statistical significance relative to untreated cells. **F** LCK expression evaluated by SYBR Green qRT-PCR in *FLT3*-ITD^{mut} MV4-11 and in *FLT3*wt THP1 cells, following 72 h of treatment with dasatinib. Data are presented as mean with SD of technical replicates. SD standard deviation. The significant fold change cut-off is depicted with a red line on the y axis. *$P \leq 0.05$, **$P \leq 0.007$.

associated immunophenotype after transplantation, further supporting the ability of *FLT3*-ITD^{mut} LPCs to recapitulate the original leukemic phenotype in vivo (Figs. 3 and S5).

Bulk blasts did not produce engraftment except for one sample, which was contaminated by LPC (Fig. S6). Secondary transplant experiments, by sorting hCD45+ cells from the BM of two engrafted mice and serially transplanting them into secondary recipients, confirmed the LPCs potential (Fig. 3C–F).

After engraftment, IF analysis of mouse BM revealed enrichment of a more immature LSC phenotype, with expansion of the CD38^{low} fraction during the second engraftment (Fig. 3B, C). Particularly, the initial engraftment revealed that 34% of hCD45+ cells were represented by LAIP+ cells (92.45% of the total CD34+ cells), with only 1.2% immature CD38^{low}/- fraction (2.05% of total CD34+ cells). After the subsequent in vivo passage, the proportion of LAIP+ cells remained comparable, accounting for 34% of hCD45+ cells (98.5% of total CD34+ cells), while the immature CD38$^{low/negative}$ fraction increased to >5% of the total hCD45+ cells

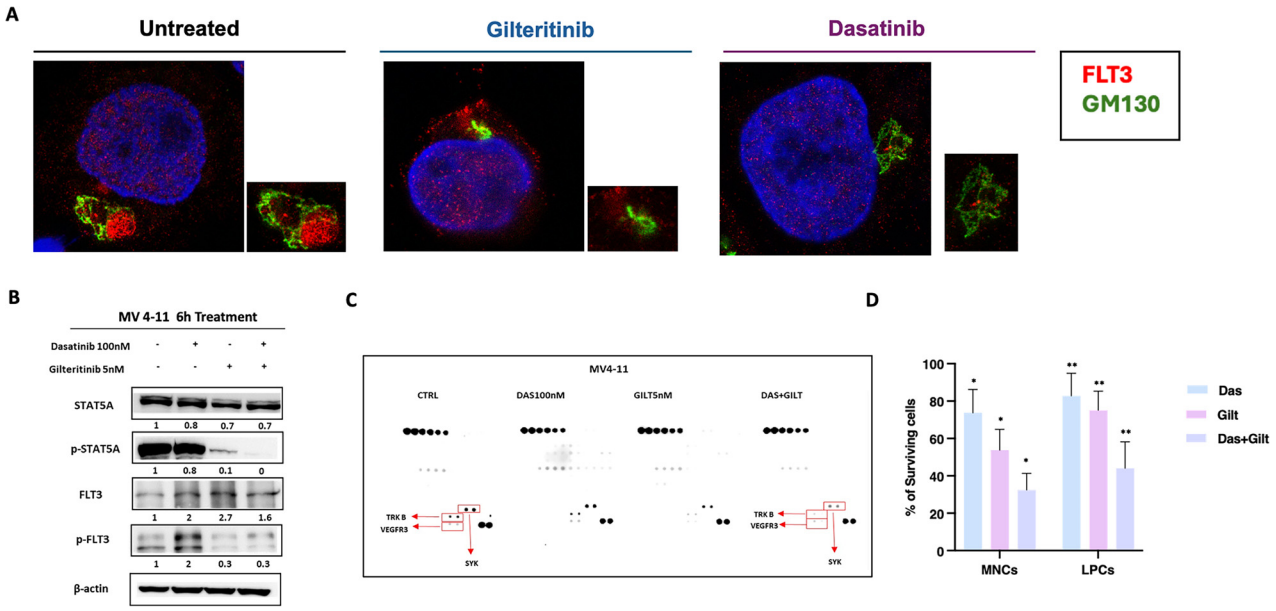


Fig. 6 Combined FLT3 and LCK inhibition disrupts FLT3/STAT5 signaling and decreases the survival of *FLT3*-ITD^{mut} AML cells. A Reduction of FLT3 expression evaluated by immunofluorescence analysis of *FLT3*-ITD^{mut} MV4-11 cells, following 24 h of treatment with gilteritinib and dasatinib. Cells were stained using anti-FLT3 (red) and anti-GM130 (green) antibodies. **B** Expression of FLT3, STAT5A, p-STAT5A, p-FLT3 protein evaluated by western blot analysis in *FLT3*-ITD^{mut} primary samples ($n = 3$), following 6 h of treatment with Dasatinib and Gilteritinib, alone or in combination. **C** Expression of phosphorylated Human receptor tyrosine kinase (RTK) proteins in MV4-11 cells treated with dasatinib and gilteritinib, alone and in combination, for 6 h, using the Human RTK Phosphorylation Antibody Array-Membrane. **D** Trypan Blue dye exclusion assay of three paired *FLT3*-ITD^{mut} AML cells ($n = 3$), after treatment with dasatinib and gilteritinib alone, and their combination for 24 h. Data are presented as means with a range of technical replicates.

(11.6% of total CD34+ cells) (Fig. 3B, C, as reported in the green panels). Capillary electrophoresis confirmed the persistence of the *FLT3*-ITD^{mut} clone after the sequential engraftments (data not shown).

Gene expression profiling of purified LPCs

To further define pathway alterations in *FLT3*-ITD^{mut} LSC, AML samples ($n = 13$) were sorted into LPC and blast fractions, and subsequently analyzed by RNA-Seq. A total of 254 differentially expressed genes (DEGs) were identified, including 236 upregulated and 18 downregulated. The DEGs are presented in a volcano plot (Fig. S7A), where the threshold corresponds to the $-\log10$ adjusted P value > 1. To investigate signaling pathways predominantly active in LPCs, we compared KEGG and Reactome pathway results. Functional enrichment of DEGs using DAVID showed the involvement of 15 upregulated (Fig. 4A), and 1 downregulated pathway (KEGG). *Focal adhesion*, *ECM-receptor interaction*, and *PI3K-Akt signaling pathway* were the most significantly upregulated in LSC versus blasts (P value < 0.05 and FDR < 0.05). Reactome pathway analysis confirmed these findings, also identifying the additional presence of common upregulated terms, including *ECM components*, *Signaling by receptor tyrosine kinases* (RTKs), and *ABC transporters*, a well-known cause of LSC multidrug resistance (MDR) (Fig. 4B) [12]. The Venn diagram in Fig. S7B reflects 22 common DEGs (42.3%) identified by the two analyses.

Using QRT-PCR, we confirmed upregulation of 30 DEGs in paired LPC and blast samples from the retrospective cohort ($n = 3$) and from an independent prospective cohort ($n = 3$) ($P < 0.0001$) (Fig. 4C). Median gene upregulation was 7 (range 2–185,878) and 40-fold (range 2–13,872), in the retrospective and prospective patient cohorts, respectively.

Targeting RTK/SFK pathways in FLT3-ITD^{mut} AML unveils a cooperative anti-leukemic effect

The enrichment of RTK signaling pathways in LPCs suggested that *FLT3*-ITD^{mut} AML progenitors may depend on RTK/SFK-mediated survival signaling [13]. To explore whether these transcriptional findings correspond to therapeutically exploitable vulnerabilities, we first tested the clinically approved FLT3 inhibitor gilteritinib, currently used for relapsed/refractory *FLT3*^{mut} AML. Consistent with its clinical activity, gilteritinib significantly reduced MV4-11 cell viability in a dose-dependent manner (Fig. 5A, B).

Among the kinases emerging from the pathway analysis, LCK drew attention as an SFK that acts downstream of RTKs and may influence FLT3 oncogenic signaling [14]. qRT-PCR performed on an extended cohort of primary AML samples ($n = 60$; *FLT3*-ITD^{mut} $n = 35$, *FLT3*^{wt} $n = 25$) and HDs ($n = 8$) revealed a fourfold upregulation of *LCK* in AML, with a sixfold increase in *FLT3*-ITD^{mut} cases (Fig. 5C).

To investigate the functional consequences of SFK inhibition, we treated MV4-11 cells and primary AML samples with the multi-kinase inhibitor dasatinib, which has activity against LCK and other SFKs. Using trypan blue exclusion assay and MTS, we evaluated the anti-proliferative and cytotoxic effects of high-dose dasatinib following treatment at 1, 10, 100 nM concentration (Fig. S10A). Interestingly, after 72 h of treatment, high-dose dasatinib (100 nM) had a significant anti-proliferative effect in *FLT3*-ITD^{mut} MV4-11, sparing *FLT3*^{wt} THP1 cells ($P = 0.03$, Fig. 5D). The anti-proliferative effect was also confirmed in *FLT3*-ITD^{mut} primary AML ($p = 0.003$) and CD34 + /CD123 + /CD25 + /CD99 + LPC samples ($P = 0.007$, Fig. 5E).

LCK inhibition perturbs FLT3/STAT5 signaling and hinders AML cell proliferation

Several studies reported that, unlike *FLT3*^{wt}, *FLT3*-ITD is mislocalized in cellular compartments other than the plasma membrane, including the Golgi apparatus, leading to autonomous oncogenic signals through STAT5 [15, 16]. Accordingly, we next examined whether LCK inhibition could influence this signaling axis in *FLT3*-ITD^{mut} AMLs.

Following 72 h of incubation of MV4-11 and THP1 cells with 100 nM dasatinib, we detected a significant reduction of *LCK* (mean: −43.41%±49.36%, Fig. 5F), and a significantly decreased expression of *FLT3* (60.94%, median FC: −2.56) and *STAT5* (61.98%, median FC: −2.63) RNA (Fig. S8B). Similar results were obtained using *FLT3*-ITD^{mut} primary AML cells, with a particularly increased effect in the LPC compartment (*FLT3*: median FC: −5.78, *STAT5*: median FC: −6.57; Fig. S8C).

Western blot analysis performed on MV4-11 cells at various drug concentrations showed a marked reduction of STAT5 phosphorylation, associated with weaker activation of FLT3 (Fig. S8D). Reduction in FLT3 protein expression was confirmed using immunofluorescence, which highlighted the inhibitory effect of dasatinib on FLT3 cytoplasmic membrane but also in the Golgi apparatus expression (Fig. 6). The same effect was observed for STAT5, whose expression was reduced in *FLT3*-ITD^{mut} MV4-11 cells after 24 h of dasatinib treatment (Fig. S9A). We next determined whether the treatment affects protein stability in MV4-11 cells, using a CHX chase assay. As shown in Fig. S8F, the half-life of both FLT3 and STAT5 proteins decreased dramatically after treatment with dasatinib.

Given the enrichment of ABC transporter genes in LPCs, we also examined whether their expression was affected by LCK inhibition. As shown in Fig. S9B, after 72 h of treatment with 100 nM dasatinib, we observed a significant reduction in the expression of ABCB1, ABCA3, ABCA6, and ABCA9 in the MV4-11 cell line and in three primary AML samples, with a selective effect in *FLT3*-ITD^{mut} cells.

Gilteritinib and dasatinib act synergistically on FLT3-ITD^{mut} AML cells

To assess potential interaction between the clinically approved FLT3 inhibitor and LCK inhibition, we combined gilteritinib and dasatinib in MV4-11 cells and primary AML samples. While dasatinib (100 nM) alone for 24 h had a limited impact at lower concentrations in terms of cell viability (Fig. S10A) and cytotoxicity (Fig. S10B), its combination with gilteritinib (5 nM) resulted in a significant reduction in cell survival and increased cytotoxicity (Fig. S10C, D). Direct comparison of treatment groups by one-way ANOVA followed by Tukey's multiple-

comparison test confirmed that the combination significantly reduced cell survival compared with gilteritinib alone (adjusted $P = 0.0326$) and dasatinib alone (adjusted $P < 0.0001$). Similarly, the MTS assay showed significantly increased cytotoxicity in the combination group compared with either gilteritinib or dasatinib alone (adjusted $P < 0.0001$ for both comparisons). The combination also enabled a significant reduction in the dose of gilteritini [17]. Interestingly, the two drugs combined induced a decrease in FLT3 and STAT5 activity already after 6 h (Fig. 6B). Moreover, looking at *RTKs signaling*, we observed a significant inhibitory effect of the combination on the kinase activity of SYK, TrkB, and VEGF3 receptors (Fig. 6C). Importantly, the anti-proliferative activity of the combination treatment was confirmed in *FLT3*-ITD^{mut} primary MNCs and LPCs isolated from three AML patients (Fig. 6D).

Discussion

Since their identification, LSCs represent a therapeutic target and a disease reservoir in AML. Several studies have identified surface markers aberrantly expressed on LSCs, and, particularly, our group previously identified a specific LAIP (CD34/CD123/CD25/CD99), associated with the presence of *FLT3*-ITD mutation [3, 18]. We demonstrated that *FLT3*-ITD^{mut} LPCs present as small clones at diagnosis, may persist after treatment, and be responsible for drug resistance and disease relapse. However, the rarity of these leukemic precursors impairs their thorough characterization, thereby hindering the development of novel and effective therapeutic strategies.

To gain deeper insight into their biological identity, we integrated MPFC and single-cell analysis on primary *FLT3*-ITD^{mut} bone marrow samples. These complementary approaches confirmed and extended our previous findings, demonstrating that the combined expression of CD34/CD123/CD25/ CD99 defines a distinct leukemic progenitor compartment specifically enriched in *FLT3*-ITD^{mut} cells. Notably, single-cell profiling revealed that CD99 expression identifies a broader population of *FLT3*-ITD^{mut} leukemic cells, including more differentiated leukemic subsets. This observation is consistent with our previous studies, indicating that CD99 alone is not sufficient to define *FLT3*-ITD^{mut} LPCs. Rather, the combined CD34/CD123/CD25/CD99 immunophenotypic signature provides the highest enrichment for the *FLT3*-ITD^{mut} compartment, while CD99 expression may also be retained in more differentiated leukemic populations.

To validate these observations in a clinically relevant setting, we prospectively analyzed newly diagnosed AML samples. MPFC demonstrated a strong correlation between the proportion of CD34^{+}/CD25^{+}/CD123^{+}/CD99^{+} cells and the presence of *FLT3*-ITD mutations, as confirmed by molecular analysis. Notably, although the *FLT3*-ITD AR was determined on bulk BM mononuclear cells, whereas the LAIP was quantified within the CD34+ compartment, the strong correlation observed supports the concept that expansion of this *FLT3*-ITD^{mut}-associated progenitor population contributes substantially to the overall leukemic mutational burden. These findings support the biological relevance of the CD34/CD123/CD25/CD99+ immunophenotypic signature as a hallmark of *FLT3*-ITD^{mut} disease.

ROC analysis identified a cut-off value of >7.4% of CD34^{+}/CD25^{+}/CD123^{+}/CD99^{+} cells within the CD34^{+} compartment as the optimal threshold for predicting FLT3-ITD positivity, with 88.2% sensitivity and 100% specificity. These findings support the incorporation of this LAIP into diagnostic workflows, in order to promptly identify *FLT3*-ITD^{mut} AML, where the addition of FLT3-inhibitors is mandatory in the context of induction chemotherapy. Moreover, the reproducibility of these findings in an independent prospective cohort further supports the robustness and clinical applicability of this immunophenotypic strategy in a real-world diagnostic setting. Importantly, as shown in our previous studies and further confirmed here using a routine diagnostic AML workflow, this immunophenotypic signature was able to identify *FLT3*-ITD^{mut} micro-clones within the leukemic population, overcoming the sensitivity limitations of conventional molecular analyses performed on bulk mononuclear cells in cases with low mutational burden. Therefore, this approach may facilitate the identification of patients who could benefit from FLT3-targeted therapies despite harboring small *FLT3*-ITD^{mut} subclones below the detection threshold of standard molecular techniques. This LAIP may also be implemented for measurable residual disease monitoring strategies in *FLT3*-ITD^{mut} AML.

To further validate the stem cell potential, sorted LPCs were injected into conditioned NSG mice, showing a higher potential to engraft and induce leukemia as compared to paired blasts, and confirming their self-renewal and

https://doi.org/10.1038/s41420-026-03319-0

Table 1 Clinical and biological features of *FLT3-ITD* mutant samples for molecular and functional studies.

Patient ID	Gender	Age (years)	Bone marrow features at AML onset			
			Blasts %	Cytogenetics	Molecular biology*	Immunophenotype
UPN1	F	73	85	46,XX[12]	*FLT3*-ITD^{mut}, *IDH2*^{mut}, *SRSF2*^{mut}, *SETBP1*^{mut}, *ASXL1*^{mut}, RUNX1^{mut}	CD45 + ,CD34 + , CD33 + , CD117 + , CD14 + , CD64 + , CD13 + , HLA-DR + , CD22 + , CD4+
UPN2	F	63	80	46,XX[12]	*FLT3*-ITD^{mut}, *NPM1*^{mut}, DNMT3A^{mut}, *TET2*^{mut}, *ABL1*^{mut}, *PTPN11*^{mut}, CEBPA^{mut}	CD34-, CD33 + , CD15 + , CD117 + , CD64 + , CD56-, HLA-DR + , CD14-
UPN3	M	51	37	Not evaluable	*FLT3*-ITD^{mut}, *SETBP1*^{mut}, CEBPA^{mut}	CD34 + , CD15-, CD117 + , CD7 + , CD13 + , HLA-DR + , CD33 + , CD45+
UPN4	F	65	87	46,X[15]	*FLT3*-ITD^{mut}, DNTM3A^{mut}, *NPM1*^{mut}, *SETBP1*^{mut}	*NA*
UPN5	M	60	62	46,X[15]	*FLT3*-ITD^{mut}, *NPM1*^{mut}, *TET2*^{mut}, *SETBP1*^{mut}, *CALR*^{mut}, CEBPA^{mut}	CD45 + , CD33 + , CD5 + , CD117 + , CD14 + , CD64 + , CD13 + , HLA-DR + , CD4+
UPN6	F	78	58	46,X[15]	*FLT3*-ITD^{mut}, *IDH2*^{mut}, *SETBP1*^{mut}, *ASXL1*^{mut}, RUNX1^{mut}	CD34 + , CD33 + , CD117 + , CD14-, CD64-, HLA-DR + , CD13 + , CD56-
UPN7	M	73	65	Not evaluable	*FLT3*-ITD^{mut}, DNTM3A^{mut}, *SETBP1*^{mut}	CD45 + , CD34 + , CD33 + , CD15 + , CD117 + , CD14 + , CD64 + , CD13 + , HLA-DR + , CD4 + , MPO+
UPN8	F	65	56	46,X[15]	*FLT3*-ITD^{mut}, *NPM1*^{mut}, *IDH1*^{mut}	*CD34-, CD33 + , CD7 + , CD15-, CD117 + , CD14-, CD13 + , HLA-DR +*
UPN9	F	54	53	46;XX,t(1;7)(q41;q22) [10]/ 46,XX[10]	*FLT3*-ITD^{mut}, DNTM3A^{mut}, *TET2*^{mut}, *NPM1*^{mut}, *SETBP1*^{mut}, CEBPA^{mut}	CD34-, CD117 + , CD13 + , CD33 + , CD7-, CD45 + , CD15-
UPN10	M	85	41	46,XY[15]	*FLT3*-ITD^{mut}, *FLT3*-TKD^{mut}, *TET2*^{mut}, *SETBP1*^{mut}, *ASXL1*^{mut}, RUNX1^{mut}	CD34 + , CD45 + , CD33 + , CD117 + , CD13 + , HLA-DR + , CD22 + , CD4 + , CD79a + , MPO+
UPN11	F	82	95	Not evaluable	*FLT3*-ITD^{mut}, *NPM1*^{mut}, DNTM3A^{mut}, *TET2*^{mut}	CD45 + , CD34 + , CD33 + , CD15 + , CD117 + , CD14 + , CD13 + , HLA-DR + , CD22 + , CD4 + , CD56 + , MPO+
UPN12	F	61	77	46,XX[15]	*FLT3*-ITD^{mut}, *NPM1*^{mut}, DNTM3A^{mut}, *ABL1*^{mut}, *SETBP1*^{mut}, CEBPA^{mut}	NA
UPN13	F	45	78	46,XX[15]	*FLT3*-ITD^{mut}, *SETBP1*^{mut}	*NA*
UPN14	F	48	58	46,XX[15]	*FLT3*-ITD^{mut}, DNTM3A^{mut}, *ABL1*^{mut}, *SETBP1*^{mut}	*NA*
UPN15	M	69	67	46,XY[15]	*FLT3*-ITD^{mut}, *NPM1*^{mut}, *CBLB*^{mut}, *TET2*^{mut}, *SETBP1*^{mut}, *KRAS*^{mut}, CE*BPA*^{mut}	*CD117 + , CD13 + , CD56 + , CD64 + , CD33 + , CD34-, HLA-DR-*
UPN16	M	58	54	46,XY[20]	*FLT3*-ITD^{mut}, *FLT3*-TKD^{mut}, *NPM1*^{mut}, DNTM3A^{mut}	*NA*
UPN17	F	73	51	46,XX[20]	*FLT3*-ITD^{mut}, *NPM1*^{mut}, *IDH2*^{mut}	CD45 + , CD33 + , CD117 + , CD13 + , HLA-DR + , CD4 + , MPO +
UPN18	F	65	56	46,XX[20]	*FLT3*-ITD^{mut}, *NPM1*^{mut}	*NA*
UPN19	M	58	53	Not evaluable	*FLT3*-ITD^{mut}, *IDH1*^{mut}	*CD34-, CD33 + , CD7 + , CD15-, CD117 + , CD14-, CD13 + , HLA-DR +*
UNP20	M	68	41	Not evaluable	*FLT3*-ITD^{mut}	*NA*
UPN21	F	62	95	Not evaluable	*FLT3*-ITD^{mut}	

Table 1 continued

Patient ID	Gender	Age (years)	Bone marrow features at AML onset			
			Blasts %	Cytogenetics	Molecular biology*	Immunophenotype
UPN22	F	36	54	46,XX[15]	*FLT3*-ITD^{mut}, *NPM1*^{mut}	CD45 +, CD34 +, CD33 +, CD117 +, CD64 +, CD13 +, HLA-DR +, CD4 +, MPO +, TDT+ NA
UPN23	M	82	62	46,XY[5]	*FLT3*-ITD^{mut}, *NPM1*^{mut}	CD45 +, CD33 +, CD7 +, CD117 +, CD13 +, HLA-DR +, CD22 +, CD4+
UPN24	F	50	78	46,XX[20]	*FLT3*-ITD^{mut}	CD45 +, CD34 +, CD33 +, CD117 +, CD13 +, HLA-DR +, CD22 +, CD4 +, CD79a +, MPO+
UPN25	F	55	64	46,XX, t(1;7)(q41;q22)[15]	*FLT3*-ITD^{mut}, *NPM1*^{mut}	*NA*
UPN26	F	45	67	46,XX[15]	*FLT3*-ITD^{mut}, *NPM1*^{mut}	*NA*
UPN27	F	51	54	Not evaluable	*FLT3*-ITD^{mut}, *NPM1*^{mut}	*NA*
UPN28	M	59	93	46,XY, t(2;13)(p22;q31)[15]	*FLT3*-ITD^{mut}	CD34 +, CD117 +, HLA-DR +, CD15-, CD33 +, CD14-, CD45+
UPN29	F	67	77	46,XX[12]	*FLT3*-ITD^{mut}, *NPM1*^{mut}	CD34-, CD33 +, CD13 +, HLA-DR +, CD7 +, CD15-, CD14-, CD64-
UPN30	M	57	78	46,XY[15]	*FLT3*-ITD^{mut}, *NPM1*^{mut}	CD117 +, CD34-, CD13 +, HLA-DR +, CD33 +, CD14 +, CD64+
UPN31	M	79	58	46,XY[15]	*FLT3*-ITD^{mut}, *NPM1*^{mut}, *TET2*^{mut}, *CBL*^{mut}	CD34-, CD33 +, CD7, CD117 +, CD14-, CD64-, HLA-DR +, CD13 +, CD56-
UPN32	M	75	51	Not evaluable	*FLT3*-ITD^{mut}	CD117 +, CD34 +, CD13 +, CD33 +, CD45 +, CD15 +, CD14 +, CD27 +, HLA-DR +, CD4 +, MPO+
UPN33	F	65	56	46,XX[15]	*FLT3*-ITD^{mut}, *NPM1*^{mut}, *IDH1*^{mut}	*CD34-, CD33 +, CD7 +, CD15-, CD117 +, CD14-, CD13 +, HLA-DR +*
UPN34	M	88	41	46,XY[15]	*FLT3*-ITD^{mut}, *FLT3*-TKD^{mut}	CD117 +, CD34 +, CD13 +, CD33-
UPN35	F	63	54	46,XX[20]	*FLT3*-ITD^{mut}, *NPM1*^{mut}	*CD117 +, CD13 +, CD34 +, CD33 +,CD7 +, HLA-DR +*

https://doi.org/10.1038/s41420-026-03319-0

leukemia-initiating potential. Interestingly, across sequential passages in mice, we observed expansion of the LPC compartment, consistent with the concept that ancestral LPCs act as reservoirs of AML persistence and resistance to AML. Moreover, the initial sorting strategy using CD99R labeling proved ineffective, probably due to CD99 masking, resulting in engraftment failure in four NSG mice, further supporting our previous evidence that CD99 plays a critical role in AML cell homing and development of human leukemic cells in the BM [15].

Despite the introduction of FLT3 inhibitors in combination with intensive chemotherapy as the standard of care for fit patients with a *FLT3*-ITD^{mut} AML, the relapse rate still remains high. This issue is even more complex in patients who are ineligible for standard chemotherapy [7, 19].

In this scenario, our study aimed at the functional characterization of *FLT3*-ITD^{mut} LPCs, and at investigating their transcriptomic profile, to identify potential therapeutic vulnerabilities. Transcriptome profiling analysis of sorted LPCs and paired blasts revealed significant enrichment of receptor tyrosine kinase (RTK) signaling, PI3K-AKT pathways, extracellular matrix interactions, and multiple ABC transporters, indicating an LSC-specific signature. Among upregulated kinases, we found overexpression of *LCK*, a member of the SRC family kinases (SFKs), which has been reported to enhance FLT3-ITD oncogenic signals through cooperation with STAT5 [10]. Consistent with transcriptomic data, LCK overexpression was confirmed in an extended series of primary AML samples, with the highest levels observed in *FLT3*-ITD^{mut} AMLs. In light of these observations, we evaluated the functional consequences of LCK inhibition using dasatinib. High-dose dasatinib significantly impaired the proliferation of *FLT3*-ITD^{mut} MV4-11 cells as well as primary *FLT3*-ITD^{mut} MNC and LPC cells, while sparing *FLT3*^{wt} THP1 cells. Interestingly, dasatinib reduced FLT3 and STAT5 transcriptional and protein levels, decreased their half-life, and markedly suppressed STAT5 phosphorylation. Importantly, dasatinib disrupted FLT3 localization not only at the plasma membrane but also in the Golgi apparatus, consistent with the previously described aberrant intracellular distribution of FLT3-ITD. In parallel, dasatinib downregulated multiple ABC transporters enriched in FLT3-ITD LPCs, suggesting a potential means of counteracting multidrug resistance mechanisms.

Building on these findings, we tested whether combining FLT3 blockade with LCK inhibition could enhance therapeutic efficacy. The combination of gilteritinib and dasatinib produced synergistic anti-leukemic effects in FLT3-ITD MV4-11 cells and primary patient samples, allowing a reduction in gilteritinib dose while enhancing apoptosis. This finding was also supported by the downregulation of kinases other than FLT3 and LCK, including TRK B, VEGFR3, and SYK. In particular, this latter receptor appears to act as a critical regulator of FLT3, involved in AML pathogenesis and resistance to FLT3 inhibitors [20], highlighting a broader cooperative inhibition of RTK/SFK signaling networks. The beneficial effect of dasatinib in combination with FLT3 inhibitors has also been reported by Patel and colleagues, who demonstrated the ability of dasatinib to overcome quizartinib resistance in *FLT3*-ITD^{mut} lines and primary cells, thereby significantly improving cytotoxicity [21]. Furthermore, we also showed that LCK inhibition may downregulate the expression of ABC transporters, which are known crucial mediators of MDR in cancer.

In summary, we characterized the *FLT3*-ITD^{mut} stem cell compartment in AML, providing the first evidence that *FLT3*-ITD^{mut} LPCs can engraft NSG mice and sustain leukemia propagation, thus functionally validating their stem cell potential. Beyond refining a clinically actionable LAIP for diagnosis and MRD assessment, our integrated transcriptional and functional analyses uncover additional molecular mechanisms underpinning LPC persistence, and identify novel therapeutically targetable vulnerabilities. Together, these findings offer a strong biological foundation for developing therapeutic strategies that selectively target residual *FLT3*-ITD^{mut} LPCs, with the aim of ultimately improving long-term outcomes in *FLT3*-ITD^{mut} AML.

Patients and methods

Patient cohort

The study cohort included 65 bone marrow (BM) samples from patients aged 19–85 years, diagnosed with de novo AML at the Laboratory of Oncohematology, Rome Tor Vergata, between 2020 and 2025, including 37 samples included as a prospective cohort. Eight BM samples from healthy individuals were included as controls. According to the declaration of Helsinki, all patients gave informed consent for the study, which was approved by the Institutional Review Board of the Policlinico Tor Vergata of Rome (NM-MY STUDY, n° 34/20, approved on February 26, 2020). Clinical and biological features of AML patients involved in in vitro and in vivo studies and molecular analyses are summarized in Table 1. The overall study cohort analysis workflow is depicted in Fig. S1.

Diagnostic work-up

Morphological, immunophenotypic, and molecular routine analyses were performed on all 65 AML cases at diagnosis. Immunophenotypic studies were performed using standard techniques, as detailed elsewhere [22].

To perform molecular and functional analyses of leukemia-associated $CD34^{+}/CD123^{+}/CD25^{+}/CD99^{+}$ cells in AML diagnostic samples, BM cells from selected cases were subsequently labeled with pre-titrated anti-human antibodies. Detailed information on staining protocols and data analysis is provided in the Supplemental material.

Patient samples positive for CD34 and for the following leukemia-associated immunophenotype (LAIP) CD99 + /CD123 + /CD25 + /CD38 + /− were chosen for transplantation into mice. LPCs and CD34−/CD3−/CD19−/CD14−/CD117 + /CD99 + /− corresponding blasts were sorted using the Astrios sorter (Beckman Coulter) without the addition of CD99R labeling. Overall, the sorted cells showed a purity greater than 98%. Representative plots of the two gating strategies used for cell sorting, depending on cell availability, are displayed in Supplementary Figs. S2 and S3.

For genetic studies, total RNA and DNA were isolated from BM mononuclear cells (MNCs) obtained by Ficoll-Hypaque density-gradient centrifugation. Genomic DNA was extracted using a column-based purification method (Qiagen, Hilden, Germany). Mutational analysis of the *FLT3* gene was performed on DNA as previously described [5]. The threshold for *FLT3*-ITD^{mut} positivity (allelic ratio AR ≥ 0.05) was defined according to the cut-off established in the RATIFY trial.

Single-cell (SC) targeted DNA library preparation and sequencing

Single-cell sequencing was performed using Mission Bio Tapestri Platform and the Tapestri Myeloid Panel (Tapestri Single-Cell DNA Myeloid Oligo Pool, *Mission Bio, Cat. MB03-0036*), following the manufacturer's instructions. Viable cells were stained with a TotalSeq™-D-Heme Oncology Cocktail (*BioLegend*, *Cat. 399906*), including CD99, encapsulated into droplets, lysed, and barcoded for single-cell DNA and protein profiling. Targeted PCR amplification and library preparation were performed according to Mission Bio protocols, and DNA and protein libraries were purified and sequenced on the NovaSeq 6000 instrument (*Illumina*). Sequencing data were processed using the Tapestri Pipeline (v3.6) for DNA, CNV, Protein analyses, and Combined Visualizations plots. Additional experimental details are provided in the Supplemental Materials.

RNA isolation and RNA-Seq

Total RNA was extracted using TRIzol™ Reagent (Invitrogen, Thermo Fisher Scientific, Waltham, MA, USA) from BM samples of *FLT3*-ITD^{mut} primary AML, and from the MV4-11 and THP1 cell lines, according to the manufacturer's recommendations, and reverse transcribed as reported elsewhere [23]. Details on RNA-Seq methodology are provided in the supplementary material session.

Validation of RNA-Seq results was performed using customized plates (TaqMan Gene Expression Array Plates; Thermo Fisher Scientific, Waltham, MA, USA), to analyze the mRNA expression levels of selected genes ($n = 30$), involved in signaling by receptor tyrosine kinase, ATP-binding cassette (ABC) transporter, and ECM component pathways. Analysis was performed on paired LPC and blast samples purified from 6 patients, 3 from the retrospective and 3 from the prospective patient cohorts. The relative quantification ($\Delta\Delta$Ct) method was used to analyze the results. The expression level of glyceraldehyde-3-phosphate dehydrogenase (*GAPDH*), a housekeeping gene, was used to normalize the expression level of our genes.

Mice model

NSG mice (NOD.Cg-Prkdc^{SCID} Il2rg^{tm1Wjl}/SzJ), 7–8 weeks of age, were purchased from Charles River. Mice were housed in separately ventilated cages with free access to food and water. Experiments started after 2 weeks of quarantine and acclimatization. All procedures were approved by the Ethical Committee (permission n°581/2021-PR). Mice ($n = 44$) were conditioned with a single intraperitoneal injection of busulfan (25 mg/kg) and transplanted 24 h later with the same amount of highly purified LPCs ($n = 29$) and paired blasts ($n = 15$) (0.5×10^6, range $0.1–1 \times 10^6$) via tail vein injection. The sample size was determined by the availability of primary patient samples providing sufficient cells for cell sorting and xenotransplantation. No randomization was used for the allocation of animals to experimental groups. Xenotransplantation was performed blinded to the identity of the transplanted cell population. Leukemia development in the engrafted mice was assessed by physical examination and peripheral blood analysis, and confirmed if the bone marrow contained more than 0.1% hCD45 cells. After engraftment, LPCs (UPN26 and UPN27) from the bone marrow of two NSG mice were purified and serially transplanted into recipient mice.

Cell cultures and in vitro treatment

FLT3-ITD^{mut} MV4-11 and the *FLT3*^{wt} THP1 AML cell lines (DSMZ, Braunschweig, Germany) were cultured in RPMI-1640 medium supplemented with 10% FBS at 37 °C in a humidified CO_2 incubator. Primary *FLT3*-ITD^{mut} AML samples ($n = 3$) were seeded in complete RPMI medium, supplemented with 20% FBS.

To assess the biological effect of Gilteritinib (ASP-2215, Selleckchem), MV4-11 and AML primary cells were seeded into 6-well plates at a density of 2×10^6 cells per well in 4 mL of complete medium, and the drug was added at increasing concentrations (1, 2, 5, and 10 nM). Similarly, the biological effect of Dasatinib (BMS-354825, Selleckchem) was evaluated under the same experimental conditions, using increasing concentrations (1, 10, and 100 nM). Subsequently, the combined effect of Gilteritinib and Dasatinib was assessed by treating cells at fixed concentrations of 5 nM and 100 nM, respectively. After treatment, cell viability was determined by Trypan-Blue dye exclusion assay (0.5% w/v) (Sigma-Aldrich, St. Louis, MO, USA) by a phase contrast microscope. Cell suspension was then collected for RNA extraction, using TRIzol™ Reagent (Invitrogen, Waltham, MA, USA) and for protein extraction, using RIPA Buffer (#9806, Cell Signaling Technology®). To evaluate the effect of dasatinib on FLT3 and STAT5 protein stability, MV 4-11 cells were incubated with 100 nM dasatinib for 1, 2, and 4 h, in the presence or absence of the protein synthesis inhibitor cycloheximide (CHX, #2112) at 100 µM. The MTT assay was performed as previously described [15]. Immunofluorescence was also used to evaluate the expression of FLT3 proteins in untreated AML cell lines (MV4-11) or after treatment with dasatinib (100 nM) for 24 h. AML cells were cytocentrifuged onto coverslips and fixed with 4% paraformaldehyde (PFA) for 10 min at room temperature, and analyzed as previously reported [15].

qRT-PCR was used for the semi-quantitative analysis of *Lck*, *FLT3*, and *STAT5* expression, by MV4-11, THP1, and primary AML cells, before and after treatment with dasatinib, using iTaq™ Universal SYBR® Green Supermix (Bio-Rad, Hercules, California, USA). Fold change was calculated using the $2^{-\Delta Ct}$ method by normalizing for *GAPDH* expression. Primer sequences are reported in Table S1.

Western blot

MV4-11 cells were treated with increasing concentration (1, 10, 100 nM) of dasatinib for 72 h and dasatinib (100 nM) and/or Gilteritinib (5 nM) for 24 h, and protein lysate from 2×10^6 cells were analyzed by western blot, as reported elsewhere [24] Incubation at 4 °C was then performed overnight with the following primary antibodies for pFLT3 (Tyr589/591) (30D4, #3464 – Cell Signaling Technology, CST), Stat5A (D2O6Y, #94205), pSTAT5A (Tyr694) (D47E7, #4322), FLT3(8F2, #3462—Cell Signaling Technology), β-actin (13E5, #4970), Vinculin (#4650). Moreover, to explore the effects of dasatinib and gilteritinib combination on RTKs signaling, we used the Human RTK Phosphorylation Antibody Array-Membrane (ab193662) following the manufacturer's instructions.

Statistical analysis

Statistical analysis was carried out using the GraphPad Prism software v8.0 (GraphPad Software, San Diego, CA). Specifically, the nonparametric Kruskal–Wallis test has been used in the evaluation of the expression data obtained from the quantitative analysis of the RNA BM samples. The Wilcoxon matched-pairs test has been used for the evaluation of the expression levels of genes of interest. Data are presented as median values derived from three independent biological replicates, each performed in technical triplicate, unless otherwise specified. GraphPad was used to evaluate synergistic drug interactions. The synergy score was calculated by Synergy Finder software (version 3.0).

Supplementary information The online version contains supplementary material available at https://doi.org/10.1038/s41420-026-03319-0.

Acknowledgements This work was supported by: Fondo Italiano per la Scienza (FIS3 – N. FIS-2024-06156); AIRC 5×1000 call "Metastatic disease: the key unmet need in oncology" to MYNERVA project, #21267 (Myeloid Neoplasms Research Venture AIRC. A detailed description of the MYNERVA project is available at http://www.progettoagimm.it); PRIN grant No. 2017WXR7ZT; PRIN grant No. 2022KRA3JF; PRIN grant No.P2022W25EA; Ministero della Salute, Rome, Italy (Finalizzata 2018, NET-2018-12365935, Personalized medicine program on myeloid neoplasms: characterization of the patient's genome for clinical decision making and systematic collection of real-world data to improve quality of health care), all to MTV; MUR-PNRR M4C2I1.3 PE6 project PE00000019 Heal Italia to MTV and ST; CG was supported by a grant from the Edward P. Evans Foundation.

Author contributions ST, TO, LB, DFA, AMV, A.V, and MTV made substantial contributions to conception, design of the study, and interpretation of the data. SA, GS, NIN, MDB, MAIC, and MD performed the experiments. MS, SM, MS, FF, and MM provided expertise and performed in vivo experiments. ML and RP helped in single-cell and RNA-Seq data analysis and performed statistical analysis. CG, FM, FB, LB, PG, AMV, and AV provided clinical data and contributed clinical expertise to data interpretation. MTV took responsibility for the integrity and accuracy of the data presented, and all authors reviewed and approved the final version of this manuscript.

Competing interests The authors declare no competing interests.

Open Access This article is licensed under a Creative Commons Attribution 4.0 International License, which permits use, sharing, adaptation, distribution and reproduction in any medium or format, as long as you give appropriate credit to the original author(s) and the source, provide a link to the Creative Commons licence, and indicate if changes were made. The images or other third party material in this article are included in the article's Creative Commons licence, unless indicated otherwise in a credit line to the material. If material is not included in the article's Creative Commons licence and your intended use is not permitted by statutory regulation or exceeds the permitted use, you will need to obtain permission directly from the copyright holder. To view a copy of this licence, visit http://creativecommons.org/licenses/by/4.0/.

References

1. Herrmann H, Sadovnik I, Eisenwort G, Rülicke T, Blatt K, Herndlhofer S, et al. Delineation of target expression profiles in CD34+/CD38- and CD34+/CD38+ stem and progenitor cells in AML and CML. Blood Adv. 2020;4:5118–32. https://doi.org/10.1182/bloodadvances.2020001742.
2. Haubner S, Perna F, Köhnke T, Schmidt C, Berman S, Augsberger C, et al. Coexpression profile of leukemic stem cell markers for combinatorial targeted therapy in AML. Leukemia. 2019;33:64–74. https://doi.org/10.1038/s41375-018-0180-3.
3. Angelini DF, Ottone T, Guerrera G, Lavorgna S, Cittadini M, Buccisano F, et al. A leukemia-associated CD34/CD123/CD25/CD99+ immunophenotype identifies FLT3-mutated clones in acute myeloid leukemia. Clin Cancer Res. 2015;21:3977–85.
4. Patnaik MM. The importance of FLT3 mutational analysis in acute myeloid leukemia. Leuk Lymphoma. 2018;59:2273–86. https://doi.org/10.1080/10428194.2017.1399312.
5. Travaglini S, Angelini DF, Alfonso V, Guerrera G, Lavorgna S, Divona M, et al. Characterization of FLT3-ITDmut acute myeloid leukemia: molecular profiling of leukemic precursor cells. Blood Cancer J. 2020;10:85. https://doi.org/10.1038/s41408-020-00352-9.
6. Perl AE, Martinelli G, Cortes JE, Neubauer A, Berman E, Paolini S, et al. Gilteritinib or chemotherapy for relapsed or refractory FLT3-mutated AML. N Engl J Med. 2019;381:1728–40. https://doi.org/10.1056/NEJMoa1902688.
7. Stone RM, Mandrekar SJ, Sanford BL, Laumann K, Geyer S, Bloomfield CD, et al. Midostaurin plus chemotherapy for acute myeloid leukemia with a *FLT3* mutation. N Engl J Med. 2017;377:454–64. https://doi.org/10.1056/NEJMoa1614359.
8. Erba HP, Montesinos P, Kim HJ, Patkowska E, Vrhovac R, Žák P, et al. Quizartinib plus chemotherapy in newly diagnosed patients with FLT3-internal-tandem-duplication-positive acute myeloid leukaemia (QuANTUM-First): a randomised, double-blind, placebo-controlled, phase 3 trial. Lancet. 2023;401:1571–83. https://doi.org/10.1016/S0140-6736(23)00464-6.
9. Krönke J, Bullinger L, Teleanu V, Tschürtz F, Gaidzik VI, Kühn MWM, et al. Clonal evolution in relapsed NPM1-mutated acute myeloid leukemia. Blood. 2013;122:100–8.
10. Marhäll A, Kazi JU, Rönnstrand L. The Src family kinase LCK cooperates with oncogenic FLT3/ITD in cellular transformation. Sci Rep. 2017;7:13734. https://doi.org/10.1038/s41598-017-14033-4.
11. Angelini DF, Ottone T, Guerrera G, Lavorgna S, Cittadini M, Buccisano F, et al. A leukemia-associated CD34/CD123/CD25/CD99^{+}immunophenotype identifies FLT3-mutated clones in acute myeloid leukemia. Clin Cancer Res. 2015. https://doi.org/10.1158/1078-0432.CCR-14-3186
12. Fukuda Y, Lian S, Schuetz JD. Leukemia and ABC transporters. Adv Cancer Res. 2015;125:171–96. https://doi.org/10.1016/bs.acr.2014.10.006.
13. Leischner H, Albers C, Grundler R, Razumovskaya E, Spiekermann K, Bohlander S, et al. SRC is a signaling mediator in FLT3-ITD- but not in FLT3-TKD-positive AML. Blood. 2012;119:4026–33. https://doi.org/10.1182/blood-2011-07-365726.
14. Kazi JU, Rönnstrand L. The role of SRC family kinases in FLT3 signaling. Int J Biochem Cell Biol. 2019;107:32–7. https://doi.org/10.1016/j.biocel.2018.12.007.
15. Travaglini S, Ottone T, Angelini DF, Fiori V, Dominici S, Noguera NI, et al. CD99 as a novel therapeutic target on leukemic progenitor cells in FLT3-ITD(mut) AML. Leukemia. 2022. https://doi.org/10.1038/s41375-022-01566-5.
16. Yamawaki K, Shiina I, Murata T, Tateyama S, Maekawa Y, Niwa M, et al. FLT3-ITD transduces autonomous growth signals during its biosynthetic trafficking in acute myelogenous leukemia cells. bioRxiv:2021;2021.01.01.424454 [Preprint] 2021. https://doi.org/10.1101/2021.01.01.424454
17. James AJ, Smith CC, Litzow M, Perl AE, Altman JK, Shepard D, et al. Pharmacokinetic profile of gilteritinib: a novel FLT-3 tyrosine kinase inhibitor. Clin Pharmacokinetics. 2020;59:1273–90. https://doi.org/10.1007/s40262-020-00888-w.
18. Travaglini S, Angelini DF, Alfonso V, Guerrera G, Lavorgna S, Divona M, et al. Characterization of FLT3-ITD(mut) acute myeloid leukemia: molecular profiling of leukemic precursor cells. Blood Cancer J. 2003;21:759–806. https://doi.org/10.1038/s41408-020-00352-9.
19. Short NJ, Nguyen D, Ravandi F. Treatment of older adults with FLT3-mutated AML: emerging paradigms and the role of frontline FLT3 inhibitors. Blood Cancer J. 2023;13:142. https://doi.org/10.1038/s41408-023-00911-w.
20. Puissant A, Fenouille N, Alexe G, Pikman Y, Bassil CF, Mehta S, et al. SYK is a critical regulator of FLT3 in acute myeloid leukemia. Cancer Cell. 2014;25:226–42. https://doi.org/10.1016/j.ccr.2014.01.022.
21. Patel AB, Pomicter AD, Yan D, Eiring AM, Antelope O, Schumacher JA, et al. Dasatinib overcomes stroma-based resistance to the FLT3 inhibitor quizartinib using multiple mechanisms. Leukemia. 2020;34:2981–91. https://doi.org/10.1038/s41375-020-0858-1.
22. Buccisano F, Maurillo L, Spagnoli A, Del Principe MI, Fraboni D, Panetta P, et al. Cytogenetic and molecular diagnostic characterization combined to postconsolidation minimal residual disease assessment by flow cytometry improves risk stratification in adult acute myeloid leukemia. Blood. 2010;116:2295–303. https://doi.org/10.1182/blood-2009-12-258178.
23. Ottone T, Silvestrini G, Piazza R, Travaglini S, Gurnari C, Marchesi F, et al. Expression profiling of extramedullary acute myeloid leukemia suggests involvement of epithelial-mesenchymal transition pathways. Leukemia. 2023. https://doi.org/10.1038/s41375-023-02054-0.

24. Banella C, Catalano G, Travaglini S, Pelosi E, Ottone T, Zaza A, et al. Ascorbate plus buformin in AML: a metabolic targeted treatment. Cancers. 2022. https://doi.org/10.3390/cancers14102565.

Publisher's note Springer Nature remains neutral with regard to jurisdictional claims in published maps and institutional affiliations.

Authors and Affiliations

Serena Travaglini[1,2] · Tiziana Ottone[1,3] · Silvia Antonelli[1] · Martina Serra[4] · Giorgia Silvestrini[1] · Silvia Masciarelli[5] · Martyna Sniegocka[5] · Nelida Ines Noguera[1,3] · Marco De Bardi[6] · Mirko Lomi[7,8] · Maria Antonietta Irno Consalvo[1] · Carmelo Gurnari[1,9] · Rocco Piazza[10] · Mariadomenica Divona[1,11] · Francesco Marchesi[12] · Francesco Fazi[5] · Maurizio Mattei[4] · Francesco Buccisano[1] · Luca Battistini[6] · Paola Guglielmelli[7] · Alessandro Maria Vannucchi[7] · Adriano Venditti[1] · Daniela Francesca Angelini[6] · Maria Teresa Voso[1,3]

1 Department of Biomedicine and Prevention, Tor Vergata University, Rome, Italy

2 Department of Experimental Medicine, University of Rome Tor Vergata, Rome, Italy

3 Santa Lucia Foundation, I.R.C.C.S., Neuro-Oncohematology, Rome, Italy

4 Interdepartmental Service Centre-Station for Animal Technology, University of Rome "Tor Vergata", Rome, Italy

5 Department of Anatomy, Histology, Forensic Medicine and Orthopedic, Section of Histology, Sapienza University of Rome, Rome, Italy

6 LIFE – Institute for Research and Health Care – Santa Lucia IRCCS, Rome, Italy

7 CRIMM, Center Research and Innovation of Myeloproliferative Neoplasms, University of Florence, AOU Careggi, Florence, Italy

8 Department of Medical Biotechnologies, University of Siena, Siena, Italy

9 Translational Hematology and Oncology Research Department, Taussig Cancer Center, Cleveland Clinic, Cleveland, OH, USA

10 Department of Medicine and Surgery, University of Milano-Bicocca, Milan, Italy

11 Saint Camillus International University of Health Sciences, Rome, Italy

12 Hematology and Stem Cell Transplant Unit, IRCCS Regina Elena National Cancer Institute, Rome, Italy

These authors contributed equally: Daniela Francesca Angelini, Maria Teresa Voso.